Hybridization of resonant modes and Bloch waves in acoustoelastic phononic crystals

Yan-Feng Wang [1], Shu-Yan Zhang,[2] Yue-Sheng Wang,[1,*] and Vincent Laude [3,†]

[1]*Department of Mechanics, School of Mechanical Engineering, Tianjin University, 300350 Tianjin, China*
[2]*Institute of Engineering Mechanics, Beijing Jiaotong University, 100044 Beijing, China*
[3]*Institut FEMTO-ST, Université Bourgogne Franche-Comté, CNRS, 25030 Besançon, France*

In phononic crystals composed of solid inclusions distributed periodically in a fluid matrix, Bloch waves are a superposition of acoustic and elastic waves coupled at the boundaries of inclusions. Resonances internal to the unit cell and localized on the solid inclusions, when present, populate the phononic band structure with additional hybridization bands. Comparing the cases of nylon in water and of steel in water, that are conveniently accessible to experiment, we relate the hybridization bands to the resonant modes, also termed quasinormal modes, of a single solid inclusion immersed in water, that are identified numerically using a stochastic excitation technique. To characterize the hybridization of the resonant modes with the continuum of Bloch waves, we compute the complex phononic band structure giving evanescent Bloch waves with acoustoelastic coupling taken into account. In the particular case of hexagonal acoustoelastic phononic crystals, we observe that the acoustic Dirac cone centered at K points of the first Brillouin zone can be severely affected without breaking the symmetry of the crystal.

I. INTRODUCTION

Mechanical waves propagating in media composed of a mixture of solid and fluid parts are superpositions of scalar acoustic waves in the fluid and of vector elastic waves in the solid [1]. Acoustic and elastic waves are coupled at every solid-fluid boundary. The number of degrees of freedom (DOF) is not the same in the acoustic domain and in the elastic domain. Acoustic waves are typically described using a single DOF, for instance, pressure, whereas elastic waves are described with up to three DOF, for instance, displacements in physical space. Solid-fluid boundary conditions are the continuity of pressure and of normal particle acceleration [2].

Phononic crystals formed from periodic solid-fluid composites are very practical for experiments [3], since a porous solid crystal or a manufactured structure are easily immersed in or filled with air or water [4–6]. Phononic crystal sensors have been proposed that use resonances of fluid inclusions inside a solid matrix [7]. The reverse case of solid inclusions in a fluid matrix has been considered extensively for demonstration of phononic band gaps [8], waveguiding [5], negative refraction [9], tunneling [10], or topological properties [11]. The appearance of local resonances in this case actually depends on the contrast between inclusions and matrix. When the matrix is air, acoustic waves feel the boundary condition on any rigid solid as almost equivalent to a fully rigid boundary condition, because of the huge impedance contrast. The problem hence reduces effectively to a single scalar acoustic wave equation only [12]. In water with heavy metal inclusions, a composition that has often been considered

experimentally, acoustoelastic boundary coupling definitely results in the excitation of elastic waves in the solid inclusion, but the effect on wave dispersion is mostly a shift of the bands, at least for frequencies up to and slightly above the first Bragg band gap [8]. For the soft inclusions of colloidal crystals [13–15] or of random composites of nylon rods in water [16,17], however, the appearance of hybridizations can be observed in the band structure already below the first Bragg band gap. Elastic resonances of the solid inclusions can indeed couple with longitudinal acoustic waves in the fluid because in-plane elastic waves have mixed shear and longitudinal polarization.

In this paper, we consider the periodic case of acoustoelastic phononic crystals. We observe that the phononic band structure is populated by additional hybridization bands for nylon in water that are absent for steel in water. Comparing both cases, we definitely relate the hybridization bands to the resonant modes, also termed quasinormal modes, of a single solid inclusion immersed in an infinite water domain. The resonant modes are identified numerically using a stochastic excitation technique [18]. To characterize the hybridization of the resonant modes with the continuum of Bloch waves, we compute the complex phononic band structure giving evanescent Bloch waves with acoustoelastic coupling taken into account. In the particular case of hexagonal acoustoelastic phononic crystals, we observe that the acoustic Dirac cone centered at K points of the first Brillouin zone can be severely affected without breaking the symmetry of the crystal.

II. BAND STRUCTURE OF ACOUSTOELASTIC PHONONIC CRYSTALS

We first consider in this section the phononic band structure and the Bloch waves of acoustoelastic phononic crystals.

_____
*yswang@tju.edu.cn
†vincent.laude@femto-st.fr

TABLE I. Mass density ρ, longitudinal velocity c_L, and shear velocity c_S for the materials considered in this paper.

	ρ (kg m^{-3})	c_L (m/s)	c_S (m/s)
Water	1000.0	1500.0	
Steel	7800.0	6023.0	3222.0
Nylon	1150.0	2396.0	932.0

This problem has been considered before, especially in the case of heavy and stiff solid inclusions in air and water [5,8]. The consideration of nylon in water, for which the shear elastic velocity is smaller than the acoustic velocity, in contrast leads to additional bands.

The scalar equation of motion for acoustic waves in the fluid can be written for the pressure as the variable as [2]

$$\frac{\omega^2}{B}p + \nabla \cdot \left(\frac{1}{\rho_f}\nabla p\right) = 0, \quad (1)$$

with B the bulk modulus and ρ_f the mass density for the fluid. This single scalar equation supplemented with rigid boundary conditions describes well sonic crystals in air.

In the case of solid inclusions in water, or whenever the contrast between the properties of fluid and solid is not overwhelming, acoustoelastic interaction must be taken into consideration. Elastodynamic motion in the solid can be described as [19]

$$\omega^2 \rho_s \mathbf{u} + \nabla \cdot (c : \nabla \mathbf{u}) = 0, \quad (2)$$

with ρ_s the mass density of the solid and c the rank-4 elastic tensor. The displacement vector $\mathbf{u}$ has three components in physical space. In this paper, we restrict our consideration to in-plane elastic waves in two-dimensional phononic crystals, so only two displacement components will be needed.

Acoustoelastic interaction can be generally described as follows. First, the normal acceleration is continuous across solid and fluid domains, leading to

$$\omega^2 \mathbf{u} \cdot \mathbf{n} = \mathbf{n} \cdot \left(\frac{1}{\rho_f}\nabla p\right), \quad (3)$$

with $\mathbf{n}$ the vector normal to the boundary. Second, the normal traction is continuous across the interface, i.e.,

$$(c : \nabla \mathbf{u}) \cdot \mathbf{n} = -p\mathbf{n}. \quad (4)$$

The phononic band structure can be obtained by combining Eqs. (1)–(4) with Bloch's theorem as outlined in Appendix A.

For concreteness we consider the two-dimensional phononic crystal whose primitive unit cell is depicted in Fig. 1(a). Cylindrical solid rods of radius r are arranged periodically according to a hexagonal Bravais lattice with lattice constant a. The filling fraction is $(2\pi/\sqrt{3})(r^2/a^2) = 0.4$. Material constants listed in Table I are specified with mass density and bulk phase velocities. The fluid matrix is chosen as water, with longitudinal phase velocity $c_L = \sqrt{\frac{B}{\rho_f}}$. Either steel or nylon are considered for the solid inclusions. For isotropic elastic solids there are only two independent elastic constants. Note that in this case $c_L = \sqrt{\frac{c_{11}}{\rho_s}}$ and $c_S = \sqrt{\frac{c_{66}}{\rho_s}}$.
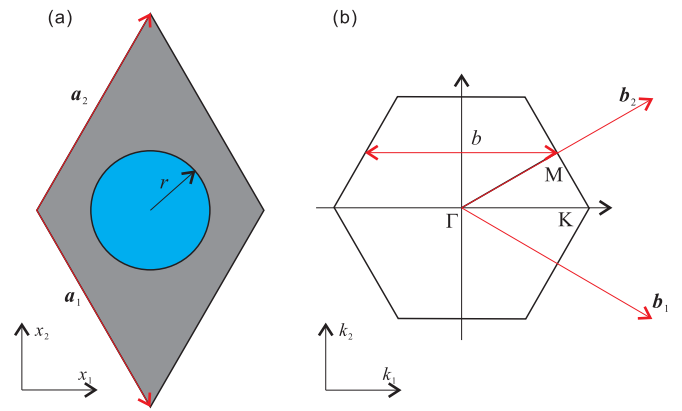

FIG. 1. (a) Primitive unit cell for two-dimensional hexagonal phononic crystals composed of solid cylindrical rods embedded in a fluid matrix. Lattice vectors are represented by the red vectors, with $\mathbf{a}_1 = a(\mathbf{i} - \sqrt{3}\mathbf{j})/2$ and $\mathbf{a}_2 = a(\mathbf{i} + \sqrt{3}\mathbf{j})/2$. (b) The first Brillouin zone is also hexagonal. High-symmetry points Γ, K, and M are indicated. $\mathbf{b}_1 = b(\mathbf{i} - \sqrt{3}/3\mathbf{j})$ and $\mathbf{b}_2 = b(\mathbf{i} + \sqrt{3}/3\mathbf{j})$ with $b = 2\pi/a$.

Band structures for steel in water and nylon in water are shown in Figs. 2 and 3, respectively. They present the reduced frequency $\omega a/(2\pi)$ of Bloch waves as a function of the wave number inside the first Brillouin zone. The band structures
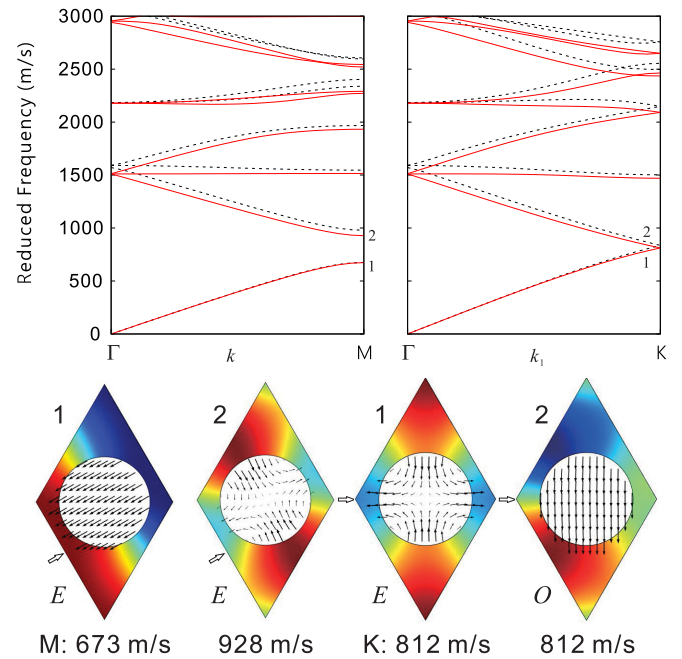

FIG. 2. Phononic band structure for a two-dimensional hexagonal phononic crystal of steel rods in water, accounting for acoustoelastic coupling. Dashed lines are for the simplified fluid-fluid case, with shear waves in the solid neglected. The first two Bloch waves at the M and K points of the first Brillouin zone are presented below the band structure. The color scale represents the pressure in water, from negative (blue) to positive (red) amplitudes. The thin arrows represent the displacement vector in the solid inclusion. The thick arrow indicates the direction of propagation of Bloch waves. The two Bloch waves at the K point are degenerate in frequency.
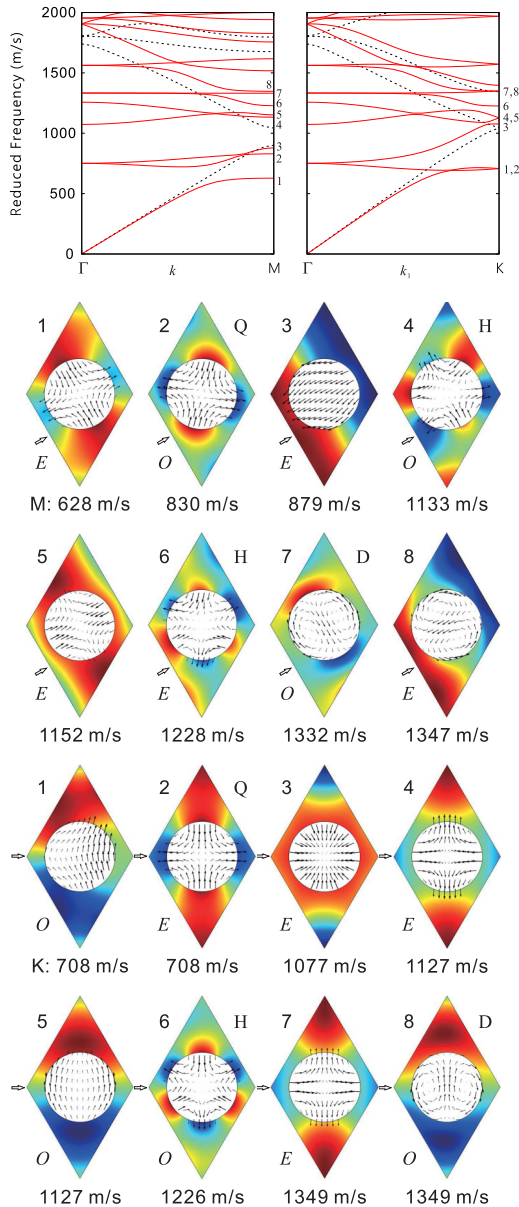
FIG. 3. Phononic band structure for a two-dimensional hexagonal phononic crystal of nylon rods in water, accounting for acoustoelastic coupling. Dashed lines are for the simplified fluid-fluid case, with shear waves in the solid neglected. The first eight Bloch waves at the M and K points of the first Brillouin zone are presented below the band structure. The color scale represents the pressure in water, from negative (blue) to positive (red) amplitudes. The thin arrows represent the displacement vector in the solid inclusion. The thick arrow indicates the direction of propagation of Bloch waves.

without acoustoelastic coupling taken into account are also presented for comparison. They are obtained by replacing the solid with an equivalent fluid having the same longitudinal velocity, i.e., neglecting the contribution of shear elastic waves. It is found that for steel in water acoustoelastic coupling does not change significantly the band structure. The main effect is a frequency down-shift of the bands, which can be understood by the fact that the shear part of the elastic energy is neglected

when acoustoelastic coupling is ignored. A Bragg gap appears for steel in water in the ΓM direction for reduced frequencies ranging between 673 m/s and 928 m/s. At the K point of the first Brillouin zone a Dirac cone is formed [20]. The first two Bloch waves at the M and K points are further presented. The first two Bloch waves at the M point have even symmetry with respect to the direction of propagation. At the K point, they are degenerate in frequency but the symmetries of the bands they form are orthogonal.

In the case of nylon in water shown in Fig. 3, in contrast, the band structure is strongly affected by acoustoelastic coupling. Comparing with the fluid-fluid band structure, it is noticed that additional bands appear. As we outline in the following section, a single nylon rod in water possesses more resonances in the low frequency range than a steel rod of identical diameter. Both the shear and the longitudinal bulk velocities of nylon are closer to the acoustic velocity of water than are the velocities of steel, and the reduced contrast favors the generation of locally resonant gaps. The Dirac cone at the K point is strongly affected as well. Actually, as we discuss later, it is pushed upward by the mixing between bands 3 and 4, counted in order of appearance from the Γ point. The first eight Bloch waves are plotted in Fig. 3 at the M and K points. They will be further discussed later in Sec. IV, once resonant modes of the rod have been introduced. For now we notice that they can be classified according to their even or odd symmetry with respect to the direction of propagation. Pairs of Bloch waves can further be degenerate at the K point. The latter situation happens for the first and the second Bloch waves, the fourth and fifth Bloch waves, and the seventh and eighth Bloch waves.

We argue in the following that the additional bands for nylon in water result from hybridization of Bloch waves with resonant in-plane polarized elastic waves that are partly trapped in the solid rods. Since the coupling of elastic waves in the rods and acoustic waves in water is significant, the surrounding water indeed creates the possibility for them to radiate energy. One resonant gap for instance appears between 628 m/s and 722 m/s for nylon in water. The Bragg gap in the ΓM direction forms between the second and the fourth bands, i.e., between 879 m/s and 1073 m/s, slightly higher than for steel in water. The up-shift of the Bragg band gap is consistent with the effective velocity of the phononic crystal in the long wavelength limit. This effective velocity is simply obtained numerically from the slope of the first band starting at the zero frequency. As a note, effective velocities for periodic elastic composites were obtained by the multiple scattering method [21] and effective velocities for periodic acoustic composites were obtained by the plane wave expansion method [22], but we are not aware of theoretical results for periodic acoustoelastic composites. The effective velocity for the nylon-in-water composite is 1672 m/s, compared to 1401 m/s for the steel-in-water composite. We have also checked that the effective velocity only increases very slightly when acoustoelastic coupling is ignored.

III. RESONANT MODES

How can we identify the resonant modes participating in the hybridizations with Bloch waves? Our idea is to obtain

first the free modes of vibration of an isolated solid rod in water. Since in-plane polarized elastic vibrations are coupled with pressure waves in water, radiation at infinity is expected. A resonant mode is also termed a quasinormal mode (QNM) in the literature [23]. In contrast to normal modes of a closed domain that are lossless, QNM has a complex resonance frequency with the imaginary part accounting for radiation loss. Because the physical domain of radiation is infinite, the practical problem of obtaining the eigenmodes is generally nontrivial. Different approaches have been proposed in the literature, for instance, based on coupling the acoustic Green's function of the infinite radiation medium to the elastic solution in the rod [24,25]. Analytical solutions for the scattering of plane waves by circular cylinders and spheres are also available [26]. However, they do not provide with the QNMs directly, but rather with their contribution to the scattering cross section as a function of frequency. Here we consider a numerical approach based on the use of a perfectly matched layer (PML) to truncate the computation domain to a finite region of space and at the same time minimize reflections from boundaries [23,27]. This approach provides us with both the frequency response and the spatial distribution of the QNMs.

The stochastic excitation technique considers a time-harmonic and spatially random body force applied to the solid rod, with zero spatial mean [18]. Appendix B summarizes the equations that are solved. Since QNMs constitute a complete basis for solutions of the time-harmonic wave equation, the response to the random excitation contains the contributions of all QNMs. In practice, the total elastic energy of the solid rod is plotted as the forcing angular frequency is tuned continuously and all resonances of the system are revealed. The responses for nylon and steel in water are plotted in Fig. 4. No resonance is observed for steel in water, whereas three distinct resonances are observed for nylon in water in the considered frequency range. The difference between steel and nylon is apparent in Table I: the shear wave velocity for nylon is smaller than the longitudinal velocity for pressure waves in water, even though the longitudinal wave velocity in nylon remains larger. In-plane vibrations of the rod have mixed shear and longitudinal displacements, leading to their partial spatial confinement. As a note, steel rods in water also support QNMs, but at frequencies larger than those considered in the band structures presented in this paper; see Appendix B.

The stochastic excitation method also provides us with approximations of the quasinormal modes when they are nondegenerate [18]. When the forcing frequency matches a resonance, the mixture of eigenmodes forming the solution indeed converges to the nearest QNM. Furthermore, the real part of the eigenfrequency is approximated by the frequency of the maximum and its imaginary part can be estimated from the quality factor of the resonance by $Q = \text{Re}(\omega)/[2\,\text{Im}(\omega)]$. The solutions at the three resonant peaks for nylon in water are illustrated in Fig. 4. Eigenmode R1 [$\text{Re}(\omega)a/(2\pi) \approx 733$ m/s; $Q \approx 14$] has quadrupolar symmetry. Eigenmode R2 [$\text{Re}(\omega)a/(2\pi) \approx 1162$ m/s; $Q \approx 21$] has hexapolar symmetry. Eigenmode R3 [$\text{Re}(\omega)a/(2\pi) \approx 1336$ m/s; $Q \approx 88$] has dipolar symmetry.

Because of the circular symmetry of the rod, the resonant modes in Fig. 4(b) can be freely rotated. If they hybridize to form Bloch waves of the crystal, however, they must respect
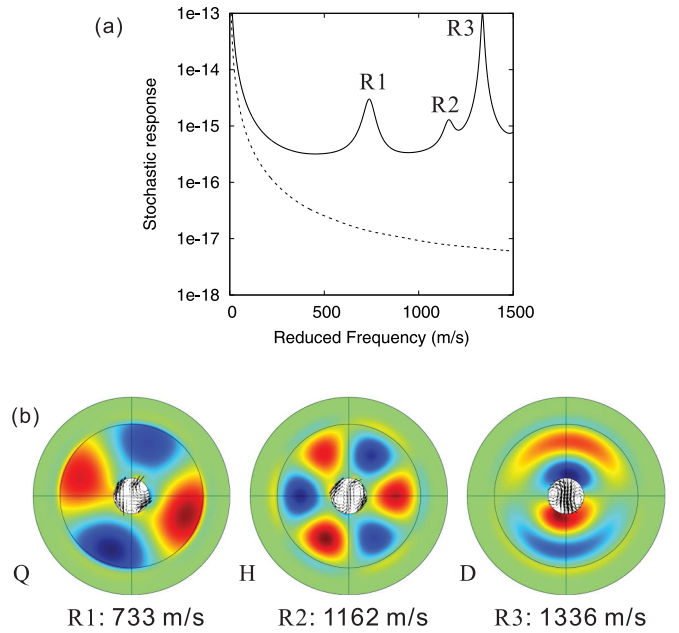

FIG. 4. (a) Stochastic response of a single nylon (solid line) or steel (dashed line) rod in water. The plot shows the total elastic energy as a function of the forcing reduced frequency $\omega a/(2\pi)$, with the lattice constant a having the same value as for the phononic crystal. (b) The resonant modes at the three resonant peaks are shown for the nylon rod. The color scale represents the pressure from negative (blue) to positive (red) maximum amplitude. The thin arrows indicate the displacement vectors. The external annular domain is the perfectly matched layer (see text). Modal symmetry is either quadrupolar (Q), hexapolar (H), or dipolar (D).

the even or odd symmetry with respect to the direction of propagation. We hypothesize that the Bloch waves in Fig. 3 can be approximated by such hybridizations with one resonant mode. Specifically, we mean that the approximation for Bloch wave BW*n* is a linear superposition of the form

$$\mathbf{u}_{\text{BW}n} \approx \alpha_{ni}\mathbf{u}_i + \beta_{nj}\mathbf{u}_{\text{R}j}, \tag{5}$$

with complex numbers α_{ni} and β_{nj} weighting the mixture of a nonresonant Bloch wave $\mathbf{u}_i$ similar to those found for steel rods ($i = 1$ or 2; see Fig. 2) and a resonant mode $\mathbf{u}_{\text{R}j}$ [$j = 1$, 2, or 3; see Fig. 4(b)]. According to such a model, the features of the resonant modes should be apparent in the Bloch waves whenever β_{nj} is not negligible compared to α_{ni}.

Applying the above classification, the Bloch waves in Fig. 3 are labeled BW*n*, $n = 1$ to 8, with increasing frequency. The symmetry (E for even; O for odd) is indicated at the bottom left corner of each distribution. The resonant mode when easily recognized is indicated at the top right corner (Q for the quadrupolar mode R1, H for the hexapolar mode R2, and D for the dipolar mode R3). At the M point, each of the resonant modes appears at most twice, for either even or odd symmetry of the Bloch wave. Furthermore, Bloch waves BW3 (respectively, BW5) look similar to nonresonant Bloch wave $\mathbf{u}_1$ (respectively, $\mathbf{u}_2$), consistently with their interpretation as entrance and exit points of the Bragg band gap. The interpretation of Bloch waves for point K is similar as for point M.

IV. HYBRIDIZATIONS IN THE COMPLEX BAND STRUCTURE

The complex band structure has been shown to be a valuable tool to study local resonances in phononic crystals and metamaterials [19,28,29]. Evanescent Bloch waves indeed form a complete basis for the solutions of the time-harmonic elastodynamic equation and the number of complex bands $k(\omega)$ is conserved as a function of frequency [30], in contrast to the classical band structure $\omega(k)$ for which the number of propagating bands generally increases with frequency. The finite element formulation we use to obtain the complex band structure considering acoustoelastic interaction is summarized in Appendix C.

Figures 5 and 6 show the complex band structures for steel in water and nylon in water in the ΓM and the ΓK directions, respectively. For comparison, the classical band structures of Figs. 2 and 3 are superimposed. As usual the real bands in the complex band structure match those of the real band structure, though flat bands are hardly caught by the $k(\omega)$ representation. The even or odd symmetry of Bloch waves is quantitatively evaluated by considering a boundary integration of the periodic pressure solution $\bar{p}_{\mathbf{k}}(\mathbf{r})$. Odd Bloch waves are also termed deaf since they cannot be excited by a symmetric plane source [31].

In the ΓM direction (Fig. 5), Bragg gaps are characterized by smooth and nonzero imaginary parts as well as constant real parts. Around the frequencies of the different resonant modes of nylon in water, however, the complex bands are varying sharply in the complex plane. For instance, a resonant gap appears around resonant mode R1 for even Bloch waves, with the lower and the upper propagating bands connected by evanescent waves with nonzero real and imaginary parts. The even propagating band holding the Bloch wave labeled A indeed interacts with the even complex band holding the Bloch wave labeled B to create that resonant gap. In contrast, the odd imaginary band holding the Bloch wave labeled C is the origin of an independent system of odd complex bands. The quadrupolar symmetry of eigenmode R1 appears clearly in Bloch wave C and continues at least up to BW2. An odd Bragg gap then opens up to BW4, at which point the hexapolar symmetry of R2 is now dominant. The next odd Bloch wave at the M point is BW7, with the dipolar symmetry of R3. As a note, the two complex bands B and C starting at the zero frequency are subdiffractive. They do not arise from frustrated orders of diffraction in the crystal [30], but because of the existence of resonant mode R1. They appear only for the first resonant mode, since the total number of complex bands is generally preserved with frequency.

Per the above discussion, it appears that in the ΓM direction resonant modes dominate the mixture described by Eq. (5) in the formation of odd Bloch waves. In the case of even Bloch waves, the mixture is more balanced in favor of the initially nonresonant propagating waves, with the exception of BW6 that clearly displays the hexapolar symmetry of resonant mode R2. Anyway, each of the resonant modes creates an even resonant band gap in the complex band structure. Since there are two independent groups of Bloch waves (even or odd), each group can hybridize independently if the (adequately rotated) free mode respects the even/odd symmetry.
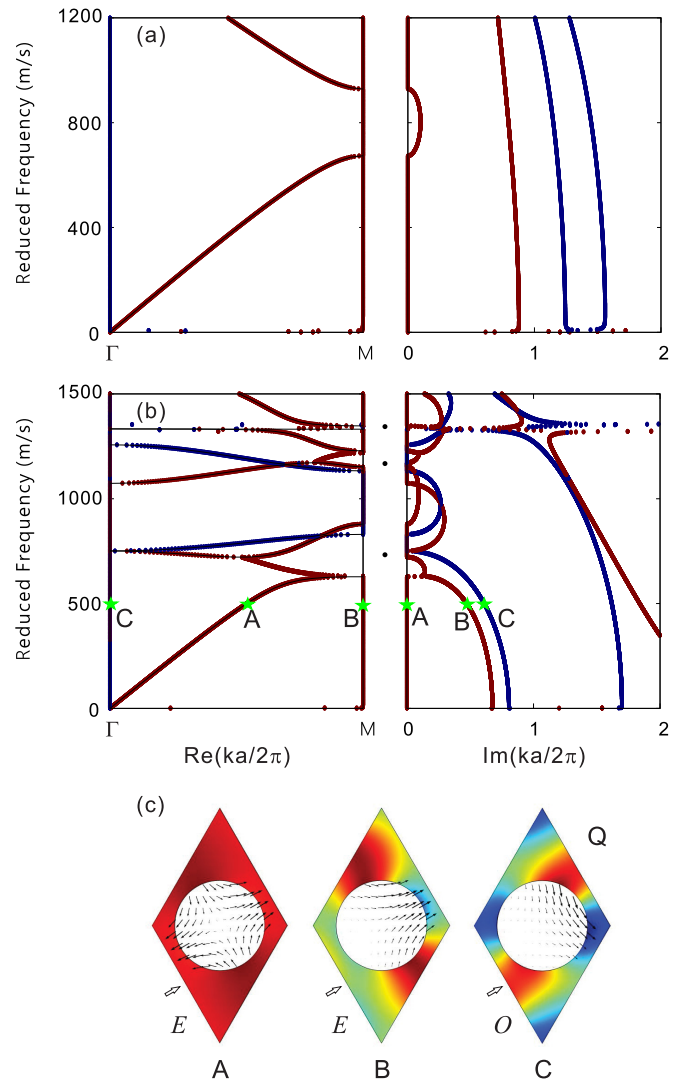

FIG. 5. Complex band structure of the two-dimensional hexagonal phononic crystal in the ΓM direction for (a) steel in water and (b) nylon in water. In either case, the left and right panels show the variation of reduced frequency versus the real or imaginary part of the wave vector, respectively. The solid lines are for the classical band structure. Even-symmetric Bloch waves appear in red; odd-symmetric Bloch waves appear in blue. The black points in between the panels of (b) mark the resonant frequencies for nylon in water. (c) Modal field patterns (periodic part only) are displayed at points A, B, and C. The thick arrows indicate the direction of propagation of Bloch waves.

In the ΓK direction (Fig. 6), similar observations can be made. We only focus on the main differences with the ΓM direction for brevity. The first nonresonant band is still even but the second one starting at the Dirac point is now odd, as the case of steel in water illustrates [8]. For nylon in water, the first resonant band gap for R1 is even, R2 induces both an even and an odd resonant band gap, and R3 induces an odd resonant band gap. The Bloch waves labeled A, B, and C now all clearly display the quadrupolar symmetry of R1. The Dirac point, originally quite close to R2, is strongly affected by the different hybridizations. The condition of a pair of degenerate
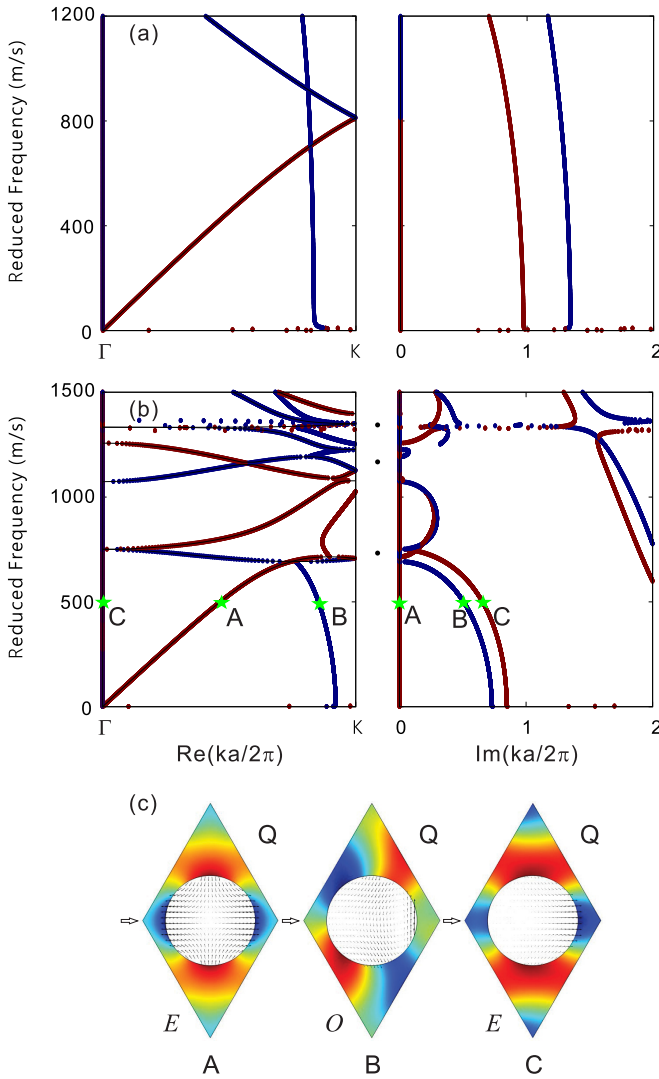
FIG. 6. Complex band structure of the two-dimensional hexagonal phononic crystal in the ΓK direction for (a) steel in water and (b) nylon in water. In either case, the left and right panels show the variation of reduced frequency versus the real or imaginary part of the wave vector, respectively. The solid lines are for the classical band structure. Even-symmetric Bloch waves appear in red; odd-symmetric Bloch waves appear in blue. The black points in between the panels of (b) mark the resonant frequencies for nylon in water. (c) Modal field patterns (periodic part only) are displayed at points A, B, and C. The thick arrows indicate the direction of propagation of Bloch waves.

Bloch waves with orthogonal symmetry is met three times, for BW1-BW2, BW4-BW5, and BW7-BW8. These points thus respect symmetry conditions similar to those of Dirac points, but they are not Dirac points since a band gap does not open concurrently along the ΓM direction.

V. CONCLUSION

We have investigated phononic crystals composed of solid inclusions distributed periodically in a fluid matrix. Taking into account acoustoelastic coupling at the boundary of inclusions, it was observed that the existence of resonances internal

to the unit cell critically affects the Bloch waves of the crystal. Indeed, the phononic band structure is populated by additional hybridization bands that are absent otherwise. The resonant modes (or quasinormal modes) of a single solid rod immersed in water were obtained by applying a stochastic excitation technique and could be recognized in certain hybridized Bloch waves. Complex band structures considering acoustoelastic coupling were obtained and were shown to characterize the hybridization process between resonant modes and the initially present nonresonant Bloch waves. In the particular case of hexagonal acousto-elastic phononic crystals considered, we observed that the acoustic Dirac cone centered at K points of the first Brillouin zone can be severely affected without breaking the symmetry of the crystal. This work could be extended to nonhexagonal and to three-dimensional acoustoelastic phononic crystals. Generally speaking, we emphasize that acoustoelastic coupling should not be neglected or overlooked in actual experiments with solid crystals immersed in a fluid matrix.

APPENDIX A: WEAK FORM OF ACOUSTO/ELASTIC WAVE INTERACTION

We consider the two-dimensional hexagonal phononic crystal shown in Fig. 1, composed of periodically arranged solid rods embedded in a fluid matrix. Waves in the fluid and solid parts are coupled at the fluid/solid interface by Eqs. (3) and (4). Acoustic waves in the fluid are governed by Eq. (1), whereas elastic waves in the solid satisfy Eq. (2). A mixed finite element formulation of the problem can be obtained as, for instance, detailed in Ref. [2]. We multiply (1) by test function p' living in the same finite element space as p and (2) by vector test function u'_i ($i = 1, 2, 3$) living in the same finite element space as u_i, and integrate independently over the fluid and the solid domains. Further applying Green's formula to both domains and inserting the coupling boundary conditions (3) and (4) leads to the coupled system

$$\omega^2 \left(\int_{\Omega_f} p' \frac{1}{B} p + \int_{\sigma} p' u_n \right) = \int_{\Omega_f} p'_{,i} \frac{1}{\rho_f} p_{,i}, \quad \text{(A1)}$$

$$\omega^2 \int_{\Omega_s} u'_i \rho_s u_i = \int_{\sigma} p u'_n + \int_{\Omega_s} u'_{i,j} c_{ijkl} u_{k,l}. \quad \text{(A2)}$$

In order to obtain the band structure, the inclusion of the wave vector dependence follows the application of Bloch's theorem. Practically, it is sufficient to make the following replacements in the pair of equations above:

$$p_{,i} = \bar{p}_{,i} - \jmath k_i \bar{p}, \quad p'_{,i} = \bar{p}'_{,i} + \jmath k_i \bar{q}, \quad \text{(A3)}$$

$$u_{k,l} = \bar{u}_{k,l} - \jmath k_l \bar{u}_k, \quad u'_{i,j} = \bar{u}'_{i,j} + \jmath k_j \bar{u}'_i. \quad \text{(A4)}$$

Equations (A1) and (A2) then form a generalized eigenvalue problem for ω^2 that can be solved as a function of **k**. The eigenvector is composed of the periodic parts of the pressure and displacement fields, $(\bar{p}, \bar{u}_i)$.

APPENDIX B: WEAK FORM FOR STOCHASTIC EXCITATION OF RESONANT MODES

In the stochastic excitation method [18], a spatially random body force **f** is applied to the solid rod so that Eq. (A2) becomes

$$\omega^2 \int_{\Omega_s} u'_i \rho_s u_i = \int_\sigma p u'_n + \int_{\Omega_s} u'_{i,j} c_{ijkl} u_{k,l} - \int_{\Omega_s} u'_i f_i. \quad \text{(B1)}$$

Equation (A1) is further modified to include a perfectly matched layer as

$$\omega^2 \left(\int_{\Omega_f} \det(J) p' \frac{1}{B} p + \int_\sigma p' u_n \right)$$
$$= \int_{\Omega_f} \det(J) J^{-t} \nabla p' \frac{1}{\rho_f} J^{-t} \nabla p. \quad \text{(B2)}$$

In this expression, J is the Jacobian matrix of a complex coordinate transform. For the cylindrical PML considered in this paper, the expression of the inverse and transposed Jacobian matrix is [2]

$$\det(J) = 1 + \frac{i}{\omega} \sigma(r) = \alpha^{-1}, \quad \text{(B3)}$$

$$J^{-t} = \begin{pmatrix} (\alpha x^2 + y^2)/r^2 & (\alpha - 1)xy/r^2 \\ (\alpha - 1)xy/r^2 & (\alpha y^2 + x^2)/r^2 \end{pmatrix}, \quad \text{(B4)}$$

with $\sigma(r)$ a loss function that is zero outside the PML and is continuously increasing inside it.

The total energy E in the solid rod is used to evaluate the response of the system and is calculated as

$$E = \frac{1}{2} \int_{\Omega_s} u^*_{i,j} c_{ijkl} u_{k,l} + \frac{1}{2} \omega^2 \int_{\Omega_s} \rho_s u^*_i u_i. \quad \text{(B5)}$$

This expression was used to plot the stochastic response of Fig. 4(a). Extending the frequency range in Fig. 7, it can be checked that the steel rod also supports resonant modes, but at higher frequencies compared to the nylon rod. The QNM at a reduced frequency of about 3600 m/s has a quadrupolar modal shape similar to that of R1. Its resonant frequencies could be decreased by increasing the radius of the rod. In a hexagonal crystal, however, the value of the radius is limited to a maximum given by the close-packing condition ($r = a/2$). Even for that radius, the frequency of the first QNM for steel in water thus remains above the Bragg band gap.

APPENDIX C: COMPLEX BAND STRUCTURE WITH ACOUSTOELASTIC COUPLING

According to Bloch's theorem, the displacement and pressure fields in a periodic system can be expressed as

$$p(\mathbf{r}) = e^{-i(\mathbf{k} \cdot \mathbf{r})} \bar{p}(\mathbf{r}), \quad u_i(\mathbf{r}) = e^{-i(\mathbf{k} \cdot \mathbf{r})} \bar{u}_i(\mathbf{r}), \quad \text{(C1)}$$
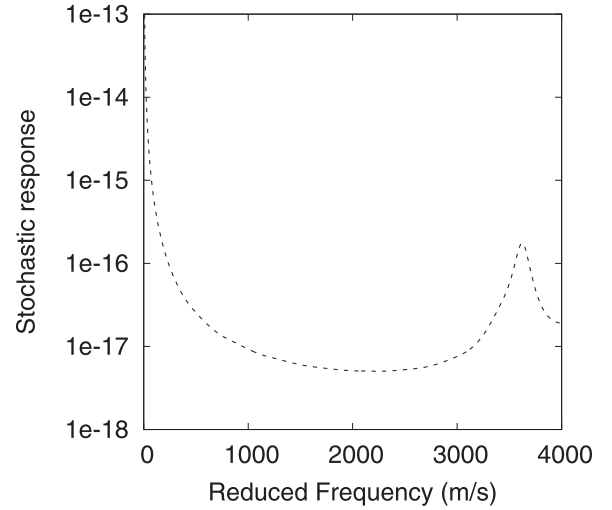

FIG. 7. Stochastic response of a single steel rod in water. The plot shows the total elastic energy as a function of the forcing reduced frequency $\omega a/(2\pi)$, with the lattice constant a having the same value as for the phononic crystal.

where **k** is the wave vector whose real part is restricted to the first Brillouin zone of the reciprocal lattice and $\bar{p}$ and $\bar{u}_i$ are periodical functions with the same periodicity as the crystal lattice. In the complex band structure, one considers a direction of propagation along unit vector $\boldsymbol{\alpha}$ and defines $\mathbf{k} = k\boldsymbol{\alpha}$ with k the (complex) wave number. The goal is to find the dispersion relation $k(\omega)$ in a given direction [30].

For both the acoustic and the elastic problem, it is useful to consider first-order differential equations of motion instead of the second-order equations (1) and (2). This consideration leads to a mixed formulation with variables $(\phi, \bar{p})$ and $(\tau_i, \bar{u}_i)$, where $\phi = -\omega^2 \boldsymbol{\alpha} \cdot \bar{\mathbf{u}}$ is the normal acceleration and $\tau_i = \alpha_j \bar{T}_{ij}$ are the stress components in the direction of propagation. Combining the weak forms for the acoustic and the elastic complex band structure leads to a generalized eigenvalue problem of the form

$$\begin{bmatrix} A_{11} & A_{12} \\ A_{21} & A_{22} \end{bmatrix} \begin{bmatrix} \phi \\ \bar{p} \\ \tau_i \\ \bar{u}_i \end{bmatrix} = ik \begin{bmatrix} B_{11} & 0 \\ 0 & B_{22} \end{bmatrix} \begin{bmatrix} \phi \\ \bar{p} \\ \tau_i \\ \bar{u}_i \end{bmatrix}. \quad \text{(C2)}$$

The block matrices A_{11} and B_{11} account for the acoustic part of the problem. They are obtained from the finite element expressions [2]

$$\int_{\Omega_f} A_{11}(\phi', \bar{p}'; \phi, \bar{p}), \quad \int_{\Omega_f} B_{11}(\phi', \bar{p}'; \phi, \bar{p}), \quad \text{(C3)}$$

with $(\phi', \bar{p}')$ vectors test functions and

$$
A_{11}(\phi', \bar{p}'; \phi, \bar{p}) = \phi'\phi + \phi'\frac{1}{\rho}(\boldsymbol{\alpha} \cdot \nabla\bar{p}) + \omega^2 \bar{p}'\frac{1}{B}\bar{p}
$$
$$
- (\nabla\bar{p}')^t \frac{1}{\rho}\nabla\bar{p}, \qquad \text{(C4)}
$$

$$
B_{11}(\phi', \bar{p}'; \phi, \bar{p}) = \phi'\frac{1}{\rho}\bar{p} - (\boldsymbol{\alpha} \cdot \nabla\bar{p}')\frac{1}{\rho}\bar{p} - \bar{p}'\phi. \qquad \text{(C5)}
$$

Similarly, the block matrices A_{22} and B_{22} account for the elastic part of the problem. They are obtained from the finite element expressions [2]

$$
\int_{\Omega_s} d\mathbf{r}\, A_{22}(\boldsymbol{\tau}', \bar{\boldsymbol{u}}'; \boldsymbol{\tau}, \bar{\boldsymbol{u}}), \quad \int_{\Omega_s} d\mathbf{r}\, B_{22}(\boldsymbol{\tau}', \bar{\boldsymbol{u}}'; \boldsymbol{\tau}, \bar{\boldsymbol{u}}), \qquad \text{(C6)}
$$

with $(\boldsymbol{\tau}', \bar{\boldsymbol{u}}')$ vectors test functions and

$$
A_{22}(\boldsymbol{\tau}', \bar{\boldsymbol{u}}'; \boldsymbol{\tau}, \bar{\boldsymbol{u}}) = (\tau')_i \tau_i - c_{ijkl}\alpha_j(\tau')_i \bar{u}_{k,l}
$$
$$
+ \rho\omega^2(\bar{u}')_i \bar{u}_i - c_{ijkl}(\bar{u}')_{i,j}\bar{u}_{k,l}, \qquad \text{(C7)}
$$

$$
B_{22}(\boldsymbol{\tau}', \bar{\boldsymbol{u}}'; \boldsymbol{\tau}, \bar{\boldsymbol{u}}) = -c_{ijkl}\alpha_j\alpha_l(\tau')_i \bar{u}_k
$$
$$
- c_{ijkl}(\bar{u}')_{i,j}\alpha_l \bar{u}_k + (\bar{u}')_i \tau_i. \qquad \text{(C8)}
$$

Coupling between the acoustic and the elastic domains occurs thanks to block matrices A_{12} and B_{21}. They are obtained respectively from the boundary integrals

$$
\int_\sigma -\omega^2 \bar{p}'\bar{u}_n \qquad \text{(C9)}
$$

and

$$
\int_\sigma \bar{p}\bar{u}'_n. \qquad \text{(C10)}
$$

---

[1] H. G. Davies, Low frequency random excitation of water-loaded rectangular plates, J. Sound Vib. **15**, 107 (1971).

[2] V. Laude, *Phononic Crystals: Artificial Crystals for Sonic, Acoustic, and Elastic Waves*, 2nd ed. (de Gruyter, Berlin, 2020).

[3] Y.-F. Wang, Y.-Z. Wang, B. Wu, W.-Q. Chen, and Y.-S. Wang, Tunable and active phononic crystals and metamaterials, Appl. Mech. Rev. **72**, 040801 (2020).

[4] R. Martínez-Sala, J. Sancho, J. V. Sanchez, V. Gomez, J. Llinares, and F. Meseguer, Sound attenuation by sculpture, Nature (London) **378**, 241 (1995).

[5] A. Khelif, A. Choujaa, S. Benchabane, B. Djafari-Rouhani, and V. Laude, Guiding and bending of acoustic waves in highly confined phononic crystal waveguides, Appl. Phys. Lett. **84**, 4400 (2004).

[6] T.-T. Wang, Y.-F. Wang, Y.-S. Wang, and V. Laude, Tunable fluid-filled phononic metastrip, Appl. Phys. Lett. **111**, 041906 (2017).

[7] R. Lucklum and J. Li, Phononic crystals for liquid sensor applications, Meas. Sci. Technol. **20**, 124014 (2009).

[8] F. L. Hsiao, A. Khelif, H. Moubchir, A. Choujaa, C. C. Chen, and V. Laude, Complete band gaps and deaf bands of triangular and honeycomb water-steel phononic crystals, J. Appl. Phys. **101**, 044903 (2007).

[9] H. Pichard, O. Richoux, and J. P. Groby, Experimental demonstrations in audible frequency range of band gap tunability and negative refraction in two-dimensional sonic crystal, J. Acoust. Soc. Am. **132**, 2816 (2012).

[10] Y. Pennec, B. Djafari-Rouhani, J. O. Vasseur, and H. Larabi, Acoustic channel drop tunneling in a phononic crystal, Appl. Phys. Lett. **87**, 261912 (2005).

[11] H. L. He, C. Y. Qiu, L. P. Ye, X. X. Cai, X. Y. Fan, M. Z. Ke, F. Zhang, and Z. Y. Liu, Topological negative refraction of surface acoustic waves in a Weyl phononic crystal, Nature (London) **560**, 61 (2018).

[12] J. Y. Lu, C. Y. Qiu, L. P. Ye, X. Y. Fan, M. Z. Ke, F. Zhang, and Z. Y. Liu, Observation of topological valley transport of sound in sonic crystals, Nat. Phys. **13**, 369 (2017).

[13] I. E. Psarobas, A. Modinos, R. Sainidou, and N. Stefanou, Acoustic properties of colloidal crystals, Phys. Rev. B **65**, 064307 (2002).

[14] T. Still, W. Cheng, M. Retsch, R. Sainidou, J. Wang, U. Jonas, N. Stefanou, and G. Fytas, Simultaneous Occurrence of Structure-Directed and Particle-Resonance-Induced Phononic Gaps in Colloidal Films, Phys. Rev. Lett. **100**, 194301 (2008).

[15] T. Still, G. Gantzounis, D. Kiefer, G. Hellmann, R. Sainidou, G. Fytas, and N. Stefanou, Collective Hypersonic Excitations in Strongly Multiple Scattering Colloids, Phys. Rev. Lett. **106**, 175505 (2011).

[16] M. L. Cowan, J. H. Page, and P. Sheng, Ultrasonic wave transport in a system of disordered resonant scatterers: Propagating resonant modes and hybridization gaps, Phys. Rev. B **84**, 094305 (2011).

[17] C. Croënne, E. J. S. Lee, H. Hu, and J. H. Page, Band gaps in phononic crystals: Generation mechanisms and interaction effects, AIP Adv. **1**, 041401 (2011).

[18] V. Laude and M. E. Korotyaeva, Stochastic excitation method for calculating the resolvent band structure of periodic media and waveguides, Phys. Rev. B **97**, 224110 (2018).

[19] Y.-F. Wang, Y.-S. Wang, and V. Laude, Wave propagation in two-dimensional viscoelastic metamaterials, Phys. Rev. B **92**, 104110 (2015).

[20] J. Mei, Y. Wu, C. T. Chan, and Z. Q. Zhang, First-principles study of Dirac and Dirac-like cones in phononic and photonic crystals, Phys. Rev. B **86**, 035141 (2012).

[21] Y. Wu, Y. Lai, and Z. Q. Zhang, Effective medium theory for elastic metamaterials in two dimensions, Phys. Rev. B **76**, 205313 (2007).

[22] A. A. Krokhin, J. Arriaga, and L. N. Gumen, Speed of Sound in Periodic Elastic Composites, Phys. Rev. Lett. **91**, 264302 (2003).

[23] C. Sauvan, J.-P. Hugonin, I. S. Maksymov, and P. Lalanne, Theory of the Spontaneous Optical Emission of Nanosize Photonic and Plasmon Resonators, Phys. Rev. Lett. **110**, 237401 (2013).

[24] J. Zhao, L. Zhang, and Y. Wu, Enhancing monochromatic multipole emission by a subwavelength enclosure of degenerate Mie resonances, J. Acoust. Soc. Am. **142**, EL24 (2017).

[25] M. K. Schmidt, L. G. Helt, C. G. Poulton, and M. J. Steel, Elastic Purcell Effect, Phys. Rev. Lett. **121**, 064301 (2018).

[26] J. J. Faran, Jr., Sound scattering by solid cylinders and spheres, J. Acoust. Soc. Am. **23**, 405 (1951).

[27] J.-P. Bérenger, A perfectly matched layer for the absorption of electromagnetic waves, J. Comput. Phys. **114**, 185 (1994).

[28] Y.-F. Wang, V. Laude, and Y.-S. Wang, Coupling of evanescent and propagating guided modes in locally resonant phononic crystals, J. Phys. D **47**, 475502 (2014).

[29] Y.-F. Wang, J.-W. Liang, A.-L. Chen, Y.-S. Wang, and V. Laude, Evanescent waves in two-dimensional fluid-saturated porous metamaterials with transversely isotropic matrix, Phys. Rev. B **101**, 184301 (2020).

[30] V. Laude, Y. Achaoui, S. Benchabane, and A. Khelif, Evanescent Bloch waves and the complex band structure of phononic crystals, Phys. Rev. B **80**, 092301 (2009).

[31] V. Laude, R. P. Moiseyenko, S. Benchabane, and N. F. Declercq, Bloch wave deafness and modal conversion at a phononic crystal boundary, AIP Adv. **1**, 041402 (2011).